Exhibit 3

analytical chemistry

University of Texas Libraries

Subscriber access provided by University of Texas Libraries

Article

Identification of Foreign Particles in Human Tissues using Raman Microscopy

Alan Campion, Kenneth J. Smith, Alexey V. Fedulov, David Gregory, Yuwei Fan, and John J. Godleski

Anal. Chem., **Just Accepted Manuscript** • DOI: 10.1021/acs.analchem.8b00271 • Publication Date (Web): 12 Jun 2018

ACS Publications

is published by the American Chemical Society. 1155 Sixteenth Street N.W., Washington, DC 20036

Analytical Chemistry

Identification of Foreign Particles in Human Tissues using Raman Microscopy

Alan Campion*[1], Kenneth J. Smith[‡], Alexey V. Fedulov[3], David Gregory[4], Yuwei Fan[5], and John J. Godleski[6†]

1. Campion Consulting, LLC, 1887 Westlake Drive, Austin, TX 78746
2. Renishaw Inc. 1001 Wesemann Drive West Dundee IL 60118
3. Warren Alpert Medical School of Brown University, Department of Surgery, Rhode Island Hospital, Providence, RI 02903
4. Pediatric Infectious Disease, Massachusetts General Hospital, Charlestown, MA, 02129
5. Electron Microscopy Facilities, Harvard TH Chan School of Public Health, Boston, MA 02115, and Boston University School of Dental Medicine, Boston, MA 02118
6. Department of Pathology, Brigham and Women's Hospital, Department of Environmental Health, Harvard T.H. Chan School of Public Health, Boston, MA 02115, and John J Godleski, MD, PLLC 304 Central Ave. Milton, MA 02186

ABSTRACT: The goal of this study was to precisely and unambiguously identify foreign particles in human tissues using a combination of polarized light microscopy and Raman microscopy, which provides chemical composition and microstructural characterization of complex materials with submicron spatial resolution. This identification for patient care and research has been traditionally studied using polarized light microscopy, electron microscopy with X-ray analysis, and electron diffraction, all with some limitations. We designed a model system of stained and unstained cells that contained birefringent talc particles, and systematically investigated the influence of slide and coverslip materials, laser wavelengths, and mounting media on the Raman spectra obtained. Hematoxylin and eosin stained slides did not produce useful results because of fluorescence interference from the stains. Unstained cell samples prepared with standard slides and coverslips produce high quality Raman spectra when excited at 532 nm; the spectra are uniquely assigned to talc. We also obtain high quality Raman spectra specific for talc in unstained tissue samples (pleural tissue following talc pleurodesis and ovarian tissue following long-term perineal talc exposure). Raman microscopy is sufficiently sensitive and compositionally selective to identify particles as small as one micron in diameter. Raman spectra have been catalogued for thousands of substances, which suggests that this approach is likely to be successful in identifying other particles of interest in tissues, potentially making Raman microscopy a powerful new tool in pathology.

The identification of foreign particulate material in tissue by pathologists for patient care and research is important because it can define unrecognized harmful exposures. Such exposures may lead to chronic diseases including cancer. Identifying foreign particulates in tissues has been approached using a number of techniques including descriptions of the appearance of the particulate material using light microscopy, the tissue response (e.g. the iron coating of asbestos fibers), the use of historical exposure information to suggest a likely identification, and the routine use of polarized light microscopy looking for distinctive features like birefringence and color as a means to help with identification[1,2]. The most detailed approach used over the last forty years involves tissue digestion, isolation of the particles or fibers, and the use of elemental X-ray spectral analysis and electron diffraction to specifically identify the materials[2,3]. The last approach has been used most widely and successfully to identify asbestos fiber types in lung tissue[3]. However, it requires a material for identification which cannot be complicated by surface contamination of specimens in the pathology laboratory. An advance to this approach used sections of paraffin embedded tissues mounted on carbon disks or paraffin blocks studied using scanning electron microscopy and energy dispersive X-ray spectroscopy[4,10]. This approach has been used when unknown particulates were observed in tissue by light microscopy (and/or polarized light microscopy) with a pathological

response and a need to identify the particulate for optimal patient care[5,6] or research[7-10]. These methods require both the specialized expertise to operate and the availability of expensive electron microscopy equipment.

The ultimate goal of this study was to unambiguously identify particles in tissues using a combination of polarized light microscopy and Raman microscopy. Particles of interest can be identified in the pathology laboratory using polarized light microscopy and the slides transferred to a Raman microscope for chemical and structural analysis. Raman microscopy and Raman spectral analysis have been used for many years in materials science and engineering to provide chemical composition and microstructural characterization of complex materials with submicron spatial resolution[11,2]. It has also been used to characterize structural features and materials in samples of biological interest, including those of clinical interest[13-15].

Talc is a common substance that may be found in human tissue because of inhalation, injection, inadvertent contamination of operative sites, and surface use[2,8]. Talc has a well-defined Raman spectrum[14] and is used in this study to develop this methodology for use by pathology services.

Our initial attempts to obtain Raman spectra from foreign particles including talc in human tissues that had been prepared using hematoxylin and eosin (H&E) stained slides failed. In the study reported here, we designed a model system that would have many of the characteristics of typical pathology tissue samples in order to explore systematically all parameters that might cause interference that would result in failure to produce acceptable Raman spectra. We examine stained and unstained samples, prepared on microscope slides and coverslips typically used in pathology as well as those made from, "white glass" and crystalline CaF_2, using several different laser wavelengths, and different mounting media. We have determined that the dominant source of interference is fluorescence from the H&E stains and demonstrate that we can obtain high quality Raman spectra from talc in our model system using standard pathology sample preparation protocols, with standard slides and cover slips, by simply eliminating the staining step. We also demonstrate our ability to obtain high quality Raman spectra from real tissue samples (pleural tissue following pleurodesis and ovarian tissue following long-term perineal talc exposure) prepared using our newly developed protocol.

EXPERIMENTAL SECTION

Cells and Tissues

Model system - To simplify this study, a model system of *in vitro* exposure of phagocytic cells to talc was used in order to have cells and particles of known composition on a slide

Cells The RAW 264.7 macrophage cell line was obtained through the ATCC. This cell line shares many properties with normal mouse macrophages and displays macrophage-specific antigens. RAW 264.7 cells have phagocytic and cytolytic properties, and can lyse tumor targets in-vitro. For maintenance, cells were cultured in 100-mm Petri dishes in DMEM with stable L-glutamine (Corning 10-017-CV) complemented with 10% fetal bovine serum, penicillin (100 units/ml), streptomycin (100 µg/ml) and 1% HEPES buffer.

Particles 10 µm and smaller sized particle grade talc ($Mg_3Si_4O_{10}(OH)_2$), CAS Registry Number: 14807-96-6, was obtained from Sigma Aldrich (Pcode 1001945014, Lot# MKBS250TV). The particles were suspended in PBS and sonicated on ice using 5 repeats of 30 second on-off cycles on maximum via the Misonix XL-2000 sonicator (Qsonica, LLC) to break up clumps.

Assay RAW264.7 cells were detached from the dish using cold PBS with 0.5% BSA, and transferred to a flat bottom non-adherent 96-well plate. Cells were exposed to talc at 10 µg/mL in 100 µL volume of PBS with 0.5% BSA and co-incubated for 2 hrs at 37 °C with 5% CO_2. The suspensions were mixed by pipetting every 30 minutes. The suspensions were then spun onto slides using a Cytospin 2 cytocentrifuge with the standard setting of 800 rpm for 5 minutes. The slides were allowed to air-dry, then fixed in 70% methanol. Three types of slides were tested including standard histology slides of normal borosilicate glass, a special "white glass" that had been purified to reduce iron content, a possible source of fluorescence, and "Raman grade" CaF_2 (calcium fluoride) that has exceptionally weak Raman scattering and which has been highly purified to eliminate fluorescence from impurities. Slides of each type were kept either unstained or stained using the standard Diff-Quick red and blue kit. Slides from each group were then either coverslipped or not using standard borosilicate glass or CaF_2 coverslips. The mounting media for coverslipping was Aqua-Mount (Lerner Laboratories).

Particles in tissues – Histology slides of a patient with known exposure to talc from a talc pleurodesis procedure from Brigham and Women's hospital and from patients with exposure by way of perineal use of talc from several other hospitals were assessed by polarized light microscopy. In cases having substantial numbers of birefringent particles, several 5 µm thick sections were cut and discarded because of possible surface talc from laboratory contamination. Subsequent sections were then mounted on slides and deparaffinized with xylene. Several different mounting media were tested for coverslipping including Permount, Cytoseal, and Aquamount. Slides without mounting media or coverslips were also studied.

The tissue blocks from these cases were also studied by scanning electron microscopy and energy dispersive X-ray spectroscopy (SEM/EDS) to determine the elemental composition of the particles using the method of Abraham and Thackral[10] for assessment of particulate materials in paraffin embedded tissue. The paraffin blocks were handled to assure no contamination of the blocks in our laboratory with talc, including handling the blocks with particle-free gloves on pre-cleaned surfaces. With a fresh surface exposed, the surface was washed in deionized water for 2 minutes to remove soluble surface materials such as sodium phosphates used in fixing and processing for histology. After air drying, the blocks were kept in a

particle-free environment until mounted for SEM examination. Block surfaces were studied with a Hitachi SU6600 field emission SEM with an Oxford EDS system, running Aztec 3.1b software. The EDS detector was an Azec X-Max 50. The backscatter mode of the microscope highlights mineral particles within the tissues. Images and spectra were acquired using 15kV accelerating voltage, 10 mm working distance, small beam spot, and objective aperture #1. Both the pleurodesis sample and the ovarian sample had magnesium silicate particles with elemental ratios consistent with talc.

Raman Microscopy

The samples were analyzed using a Renishaw inVia Raman microscope with a Peltier-cooled Centrus CCD detector and MS20 encoded stage with 100 nm step resolution. (Renishaw, Wotton-under-Edge, UK). The microscope was equipped with a 50 mW 532 nm laser; typical power at the sample using the 10% setting was 3 mW. We conducted a few preliminary experiments using other lasers but we do not report them here as they offered no significant advantages over 532 nm. Calibration of the instrument was performed with an internal neon source and checked periodically by measuring the frequency of the 520 cm^{-1} line of a Si(100) wafer. Dispersion was 2.75 cm^{-1} per pixel for the 1200 lines/mm grating and 1.19 cm^{-1} per pixel for the 2400 lines/mm grating. Acquisition times for individual particle analysis varied from 10 to 120 seconds and the number of accumulations added together varied from one to five. Spectra were collected using a 50X magnification objective (NA 0.75). Renishaw WiRE software was used for data acquisition and analysis.

RESULTS AND DISCUSSION

Model System Results – Unstained Samples

Figure 1 shows photomicrographs of the stained and unstained samples of the RAW264.7 cell macrophage preparations. The left panel shows macrophages with small (~5 μm and smaller) birefringent particles in a hematoxylin and eosin stained slide highlighted with partially polarized light. Note the presence of small particles within and on the surface of macrophages as well as that of free particles. The right panel shows the polarized light image of an unstained cytocentrifuge preparation from the same experiment, showing small birefringent particles. The outlines of cells can be seen by direct microscopy and are also visible in the photomicrograph of the unstained sample. Importantly, the birefringent particles are clearly observed to be in the same size range with similar size distributions in both preparations. Identification of particles by size, shape, and cell association are important features when performing Raman spectroscopy on unstained sections. Figure 2 shows the Raman spectrum of a single talc particle from the unstained sample, along with that of talc obtained from a database of mineral Raman spectra.[14]

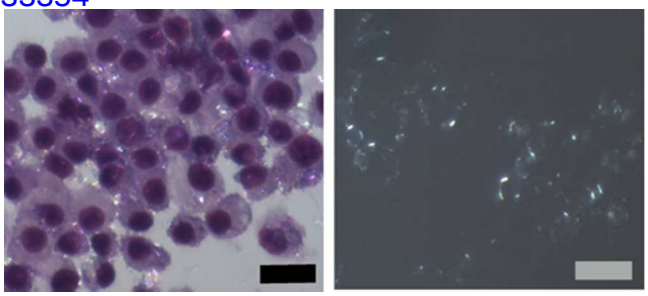

Figure 1. Photomicrographs of RAW 264.7 macrophage cells in cytocentrifuge preparations. The left image is that of a standard H&E stained preparation examined under partially polarized light. The right image is that of an unstained sample examined under partially polarized light. These slides were coverslipped using Aquamount, and then analyzed by Raman spectroscopy. Original magnifications for both panels 400X; Bar on both panels = 20 μm.

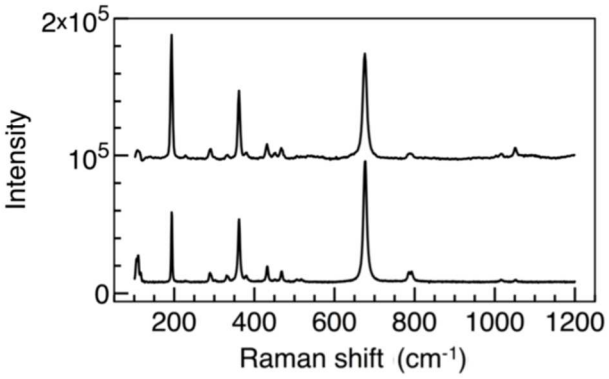

Figure 2. The Raman spectrum of a single talc particle from the unstained sample (top) along with the Raman spectrum of talc taken from a reference library (bottom).[16] The top spectrum was taken using the lower resolution 1200 lines/mm grating and the spectral range was chosen to match that of the reference spectrum.

The Raman spectrum from the unstained sample was obtained by subtracting the background Raman scattering and fluorescence of the glass slide, cover slip, and mounting medium from the raw data; a baseline correction was also applied. The spectrum, which was obtained in about 10 minutes, has a very high signal-to-noise ratio due to the lack of interference from background fluorescence. We chose this particular reference spectrum because this talc sample appeared to be remarkably free of impurities, as judged by comparison with previous work and theoretical calculations[17-19], and by comparison with samples from other databases.[20,21].

Not surprisingly, the frequencies and relative intensities observed are nearly identical in the two spectra because we prepared our model system to include reagent grade talc particles. The frequencies match the reference frequencies to better than ± 1 cm^{-1} (see Table 1) and the relative intensity patterns are essentially identical. We have not included the OH stretch, which appears at 3667

cm^{-1}, both in our spectrum and that of the reference, not only to make the table readable but also because we don't consider it further; it seems not to contribute any significant information to the analysis not carried by the lower frequency region.

Table 1. Comparison of Raman shifts from a talc particle in the unstained sample (AF – 3-13), along with that from a database of mineral Raman spectra, and mode assignment to be discussed later. The most intense bands are identified in bold type.

Sample	Raman Shifts (cm^{-1})								
AF 3-13	109	**192**	291	**361**	431	467	**676**	787	790
Ref.[16]	109	**193**	288	**361**	431	467	**676**	785	792
Mode[19]	6	10	14	22	30	36	42	49	51

Talc Structure and Raman Spectrum

Talc is a trioctahedral sheet silicate (a member of a class of phyllosilicates) with chemical composition $Mg_3Si_4O_{10}(OH)_2$ and its Raman spectrum[17-19], along with those of other silicates, including phyllosilicates is well understood[20]. The trioctahedral (TOT) structure consists of a positively charged octahedral layer sandwiched between two negatively charged tetrahedral silicate layers. The octahedral layer is often referred to as the "brucite" layer by analogy to the mineral brucite with the molecular formula $Mg(OH)_2$. The talc sheets are weakly bonded to one another by van der Waals forces, allowing them to glide past each other quite easily, like the planes in graphite, which accounts for the softness of talc. It is, in fact, the softest known mineral and has been assigned the value 1 on the Mohs hardness scale. Figure 3 shows a portion of the structure of one of the talc sheets, viewed along the *c* axis. Some of the silicate groups have been omitted for clarity.

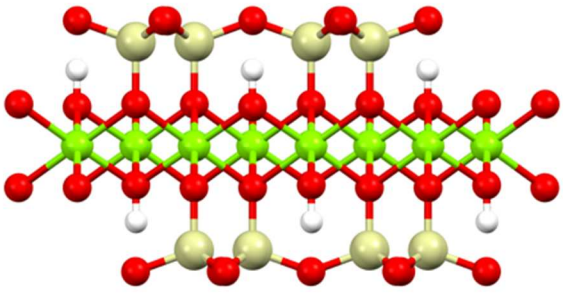

Figure 3. The structure of talc, viewed along the c axis. The octahedral coordination of Mg^{2+} (green) is clearly shown in this view, as is the tetrahedral coordination of Si^{4+} (grey). Bridging oxygen atoms are red and hydrogen atoms are white.

Table 1 shows the Raman shifts and mode assignments made using first principles DFT calculations[19]. The motions described here were informed by animations of the simulations kindly provided by the authors of Ref. 19 and are used to identify the atomic displacements involved. One or more modes may have approximately the same frequency (degeneracy) but we have chosen to identify them by a single frequency because the motions involved are so similar.

We describe the vibrational modes of talc with reference to its molecular structure shown in Figure 3. These modes have been assigned as follows[19]: Modes 6 (and 7), appearing as an unresolved band centered around 109 cm^{-1}, are shearing motions in which the covalently bonded tetrahedral silicate layers can be thought of as sliding laterally back and forth, out of phase with one another, with respect to the "brucite" layer. Mode 10, the strong mode that appears at 193 cm^{-1}, can be thought of as a stretching or breathing motion of the TOT structure, in which the tetrahedral layers move up and down (perpendicular to) the brucite layer. As far as we have been able to determine, this mode is unique to talc. Mode 14, at 288 cm^{-1}, is assigned as a Si-O-Si bending motion, analogous to a similar motion in silica, SiO_2. Mode 22, at 361 cm^{-1} is attributed to the stretching of Mg-OH bonds perpendicular to the plane of the brucite layer. It can be thought of as a symmetrical stretch involving an OH group bonded to three Mg^{2+} ions. Modes 30 (at 431 cm^{-1}) and 36 (at 467 cm^{-1}) are Mg-OH and Mg-O stretching motions, respectively. Mode 42 (676 cm^{-1}) is the symmetric silicate stretching mode. Modes 49 (785) and 51 (792) are assigned as Si-Si modes that involve bending and stretching of the Si-O-Si bonds parallel to the plane of the "brucite" layer. Mode 62, the O-H stretch, appears at 3667 cm^{-1}. These assignments are summarized in Table 2.

Table 2 Talc mode assignments from DFT calculations

Mode	**Assignment**
6	TOT layers lateral shearing
10	TOT layers vertical breathing
14	Si-O-Si bend
22	"brucite" Mg-OH stretch
30	Mg-OH stretch
36	Mg-O stretch
42	Symmetric silicate stretch
49	Si-Si combination bend and stretch
51	Si-Si combination bend and stretch
62	O-H stretch (not shown)

Model System Results – Stained vs. Unstained Samples

Figure 4A shows that the signal from a particle in an (H&E) stained sample is dominated by intense fluorescence from the colored dyes; there are no observable

peaks in the spectrum that can be assigned to the Raman spectrum of talc. Raman scattering cross sections are about ten orders of magnitude weaker than fluorescence cross sections so the Raman signal must be equal to or larger than the noise in the fluorescence signal in order to be detected. Figure 4B illustrates the difficulty involved. We have superimposed the 675 cm^{-1} peak from the Raman spectrum of a particle in the unstained sample on an expanded view of the spectrum from taken from a particle in the stained sample. (These particles are "typical" and not necessarily the same as those from which the spectra in Figures 2 and 4A were obtained.) We chose to focus on the region near the 675 cm^{-1} band to minimize difficulties with background subtraction and scaling. Differences in laser power and signal integration times were taken into account to make the vertical scales the same. In addition, we applied an offset to the stained spectrum so that the range would be the same as that for the unstained spectrum. The zero shown on the *y*-axis is arbitrary; only the range is significant. Figure 4B shows that the signal from one of the strongest bands in the Raman spectrum of a talc particle in the unstained sample would be buried in the noise from the fluorescence background in the stained sample and would therefore be undetectable.

It is not possible to make a general estimate of signal-to-noise ratios to be expected in these experiments involving stained samples because: 1) The Raman signal intensity depends upon the size and orientation of a talc particle; and 2) The background fluorescence intensity depends upon the concentration of the stain surrounding that particle, which is by no means uniform throughout a particular sample. An order of magnitude estimate, however, using our data, illustrates the difficulty posed by competing fluorescence. The signal-to-noise ratio (SNR) for the present problem can be estimated by identifying all noise sources and making the usual assumption that noise adds in quadrature. The SNR is then calculated using the formula $\mathrm{SNR} = S/N = S/\sqrt{S+B+D}$, in which S represents the signal intensity, B the intensity of the background fluorescence, and D any noise associated with the detector. The 675 cm^{-1} peak intensity in the Raman spectrum from talc particles in unstained samples we have examined is of the order of 10^4 counts whereas the fluorescence intensity from talc particles in stained samples is of the order of 10^{10} counts, at comparable laser power and signal integration times. We can ignore contributions to the noise from the signal itself and the detector because they are smaller than the background intensity by orders of magnitude. $B >> S+D$ so $\mathrm{SNR} \approx S/\sqrt{B} = 10^{-1}$, which is about what we see in Figure 4B. We emphasize that this example is "typical" in the sense that we have tried to obtain Raman spectra from a number of talc particles in a number of matrices that have been stained with standard H&E dyes without success. While the background fluorescence varied from sample to sample by a factor of ten or so, it was still many orders of magnitude stronger than the Raman spectrum of talc, which explains why we have been unable to obtain Raman spectra of talc from stained samples.

Having demonstrated that we can obtain high quality Raman spectra of talc in a biological matrix it becomes important to establish the reproducibility of our measurements and to demonstrate that the assignment of these spectra to talc is unequivocal. We have chosen to focus only on the three most intense bands for the present purpose. We have measured the Raman shifts of these bands in five particles from this sample and find that the reproducibility of the frequencies from particle to particle is remarkable. Means and standard deviations are: 191.0 ± 0.55 cm^{-1}, 359.2 ± 0.45 cm^{-1}, and 673.8 ± 0.45 cm^{-1}. Applying Student's t-distribution to the 359.2 cm^{-1} data shows that the 99% confidence interval is achieved for an uncertainty of ± 1 cm^{-1}. We found this degree of reproducibility to be surprising at first but can rationalize it as follows. These talc particles are relatively large, of the order of 1 – 10 μm in diameter, which has two important consequences: 1) They are likely to be single crystals, as shown by their birefringence, with very little dispersion in their phonon frequencies and 2) The surface area to volume ratio is small, making interactions with the surrounding matrices unimportant.

The assignment of these spectra to talc is unequivocal. Searching multiple databases[16,21,22] for minerals with a peak near (± 2 cm^{-1}) 191 cm^{-1} returns only one hit, talc. There are four minerals with a peak near 359 cm^{-1}, one of which is talc, and there are three minerals with a peak near 675 cm^{-1}, one of which is talc. We can make a conservative estimate of our confidence level in an alternative way; we can simply assume that we are only 95% confident in each of the peak assignments, despite the higher confidence demonstrated above. Treating the probabilities of finding these three peak frequencies as independent of one another we estimate the odds of these particles not being talc is no greater than $(0.05)^3 \approx 10^{-4}$.

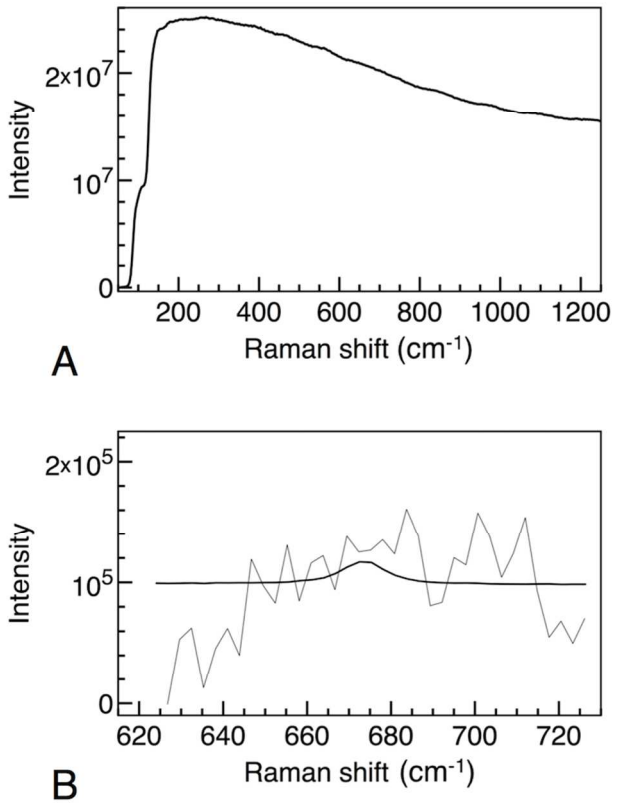

Figure 4A. The Raman spectrum taken from a talc particle in the stained sample, which is dominated by fluorescence from the biological stains. **4B**. Raman spectra of a talc particle in the unstained sample (darker line) compared with that of a talc particle in the stained sample (lighter line). The spectra have been scaled with respect to laser power and integration times and offset for clarity.

Particles in Tissues

Our model system facilitated the controlled assessment of multiple parameters that might influence the ability of Raman spectroscopy to identify particles associated with cells. Questions remained as to whether or not more complex tissues might in some way affect the Raman signal, especially tissues with birefringent type 1 collagen or other features such as red blood cells or tissue products with iron containing proteins. In addition, we sought to assess the utility of the technique in identifying talc particles of different sizes. Two different kinds of tissues prepared from paraffin tissue blocks were tested in order to address these questions: 1) A talc pleurodesis sample with red cells, hemosiderin, foreign body granulomas, giant cells, dense collagenous tissues and large talc particles, all greater than 10 μm; and 2) Ovarian stromal tissue with adjacent high grade serous ovarian cancer tissue from a woman with long-term perineal talc use and small particles within the stroma and tissue macrophages. Although a variety of particle sizes were examined in the model system, we sought to assess our ability to obtain Raman spectra from both larger (> 10 μm) and smaller (< 10 μm) particles in these more complex biological matrices. Talc particles in ovarian tissue samples that result from perineal talc use, in particular, are known to fall in to the lower size range.

We made an interesting and important discovery when we examined these samples. Several sections were mounted using Permount, because of its widespread use in pathology labs, and others were prepared using Cytoseal and Aquamount, for comparison purposes. We were unable to obtain any acceptable spectra from samples mounted using Permount, due to the presence of both broad fluorescence and some structured peaks, presumably due to Raman scattering from the Permount itself. Permount is a slightly yellow liquid that absorbs in the blue-green region of the spectrum and emits fluorescence over our spectral region of interest. Samples mounted using Cytoseal gave acceptable results as shown below, but required background subtraction. We initially preferred Aquamount as the mounting medium of choice for these applications because it has the least interference and because coverslips can be sealed with clear nail polish. Re-examining some of these slides after a few months showed that bubbles had developed, presumably due to evaporation, and we are currently re-evaluating Cytoseal as our medium of choice.

Figure 5 shows polarized light images of sections of pleural tissue, following talc pleurodesis with large particles, in a (H&E) stained section as well as an unstained section. Multinucleate giant cells, red blood cells, and a fibrotic tissue response were present along with the large birefringent talc particles; all of these characteristics were also observed in the unstained section. The left panel illustrates multinucleate giant cell tissue response and presence of birefringent particles in a routine (H&E) stained slide highlighted with partially polarized light. The right panel illustrates the polarized light examination of an unstained deeper section from the same block showing large (~20 μm in greatest dimension) birefringent particles. This slide was dipped in xylene to remove paraffin, coverslipped using Cytoseal, and then analyzed by Raman spectroscopy.

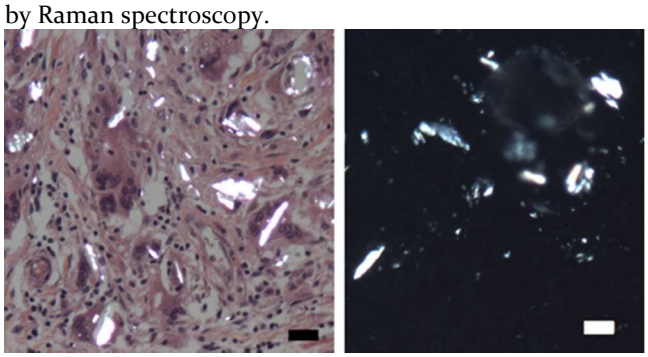

Figure 5. Photomicrograph of pleural tissue following talc pleurodesis with large particles. The left image is that of a standard H&E stained preparation examined under partially polarized light. The right image is that of an unstained sample examined under partially polarized light. Original magnifications for both panels 200X; Bar on both panels = 20 μm.

Figure 6 shows the Raman spectrum of a talc particle embedded in one of our lung pleurodesis samples. The frequencies as well as the relative intensities observed (see Figure 2) clearly identify this particle as talc. We sampled five particles in two different samples and found that the frequencies were nearly identical. Means and standard deviations for the five particles' frequencies were: 191.4 ± 0.9 cm^{-1}, 359.4 ± 0.55 cm^{-1}, and 673.4 ± 0.45 cm^{-1}. In addition to establishing our ability to obtain Raman spectra from talc in a "real world" sample, these data show how remarkably insensitive the spectral shifts are to the nature of the biological matrix when large particles, greater than 10 μm, are assessed. Not only are these pleural tissue samples significantly different from those of our model system, the data shows excellent reproducibility among spectra from several different particles in two different slides.

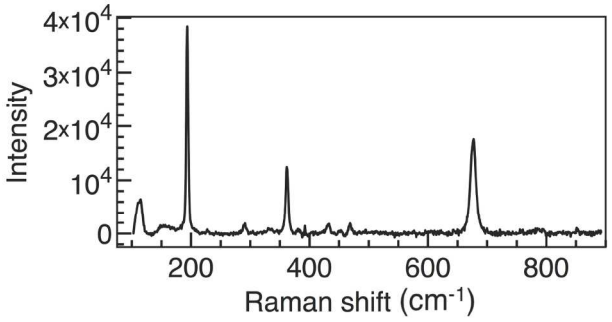

Figure 6. Raman spectrum of a talc particle in an unstained sample of pleural tissue following talc pleurodesis. This spectrum was taken with the 2400 lines/mm high-resolution grating, which produces sharper lines but over a more restricted spectral range than the spectra of talc particles in our model system

Although many pathologists have little experience in studying unstained slides with polarized light microscopy, most slides with foreign particles have distinctive geographic features which are also highlighted by polarized light and can be used for orientation on the slide. Examples of unstained features visible with polarized light include fibrous tissue, blood vessels, granulomas, and giant cells[1]. In most cases, the birefringent foreign particles of interest are considerably brighter than the visible structural features of the tissues. Experience in interpreting these unstained preparations is quickly and easily acquired. One of the few artifacts of these preparations is the incomplete removal of paraffin which can leave behind birefringent artefactual structures, so complete removal of paraffin with xylene is important. Although this protocol does not permit the analysis of the specific particles seen on the stained slide, pathologically significant particles are very likely to be found on additional sections of the same block which has been the longstanding concept as the basis of many pathological analyses [2,3,4].

Figure 7 shows sections of ovarian tissue from a woman with a history of perineal talc use, with many ~5 μm and smaller birefringent particles in macrophages in a focus of fibrous tissue in ovarian stroma with hematoxylin and eosin stain. The left panel illustrates macrophages in a focus of fibrous tissue with many small (~5 μm and smaller) birefringent particles in a routine H&E stained slide highlighted with partially polarized light. Note the lack of giant cells and the presence of these small particles within macrophages and fibrous tissue. The right panel illustrates the polarized light examination of an unstained deeper section from the same block showing small birefringent particles. This slide was dipped in xylene to remove paraffin, coverslipped using Cytoseal, and then analyzed by Raman microscopy. Ovarian tissues with high grade serous ovarian cancer are not shown in the figure, but are located adjacent to the field illustrated. Both the ovarian and cancer tissue are different in structure from that in Figure 5, yet it was possible to find the birefringent particles with polarized light examination of an unstained deeper section from the same block and carry out Raman microscopy.

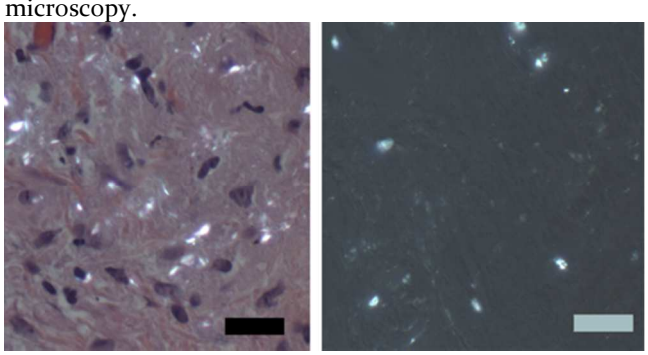

Figure 7. Photomicrograph of ovarian tissue from a woman with a history of perineal talc use showing many small particles. The left image is that of a standard H&E stained preparation examined under partially polarized light. The right image is that of an unstained sample examined under partially polarized light. Original magnifications for both panels 400X; Bar on both panels = 20 μm.

The Raman spectrum of a talc particle in this section is shown in Figure 8. We were not able to take a calibrated photomicrograph of this particular particle under polarized light using the Raman microscope but under white light it appeared to be roughly cylindrical in shape with dimensions ca. 2 μm x 5 μm, which is representative of the particle observed in the ovarian tissue samples. Several peaks not assignable to talc (521 cm^{-1} and 814 cm^{-1} for example) are present in the broad background taken from a location adjacent to the particle and are due to Raman scattering from the Cytoseal; their presence in the subtracted spectrum reflects compromises we chose in scaling to get the best overall result. The broad background also contributes to the higher level of noise observed in this spectrum relative to others. We looked at six particles and found identical frequencies, 194 cm^{-1}, 362 cm^{-1}, and 676 cm^{-1}.

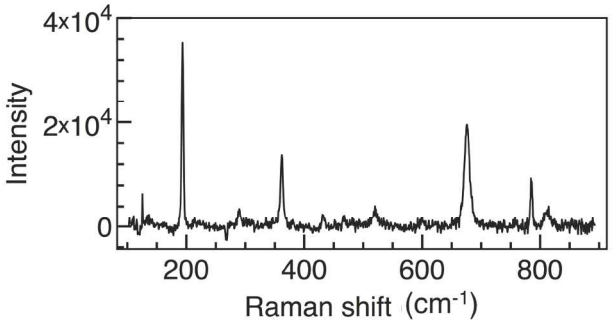

Figure 8. Raman spectrum of a talc particle in an unstained sample of ovarian tissue from a woman with a history of perineal talc use. This spectrum was taken with the 2400 lines/mm high-resolution grating, which produces sharper lines but over a more restricted spectral range than the spectra of talc particles in our model system.

To put this advance into clinical practice, particles can be identified in deparaffinized, unstained, and coverslipped tissue on slides by any experienced pathologist using polarized light microscopy and further analyzed by Raman microscopy either in their laboratory or in a specialized Raman microscopy lab. If a specialized lab is used, the referring pathologist can send both stained and unstained slides or use a slide with a calibrated grid[23] as a means to be sure the correct particles are analyzed. The coordinates of the particles of interest, determined using a calibrated grid, can be transferred along with the sample slide to the Raman microscopy lab so that the particles of interest can easily be identified for further study. We have no reason to believe that our protocol would not be successful in identifying other particles of interest although we will have to test this hypothesis by studying other foreign materials in human tissues to determine if the protocol we have developed here will be generally applicable. Because Raman spectroscopy is already in use for clinical applications on living tissues *in situ* via endoscopy and on the skin surface to differentiate normal and malignant tissues as recently reviewed[13], our findings have the potential to expand this area of inquiry to tissues removed at surgery and thereby extend use of Raman spectroscopy not only for characterizing tissues, but also to relating unique Raman patterns to outcome and prognosis which could be another important clinical advance.

CONCLUSION

We have demonstrated our ability to unambiguously identify talc particles in a model system and in tissues using Raman microscopy. The key to success was the elimination of the staining step in the standard pathology sample preparation protocol. This study provides a protocol for tissue analysis of foreign particulates important in the development of the disease process for which the tissue was removed. Detailed testing of materials used in histological preparation of tissue slides and identification of specific choices among acceptable materials and those to avoid is particularly valuable for the practical adaptation of this advance. We also offer suggestions for optimal collaboration between hospital pathologists and Raman microscopy reference laboratories. Our findings suggest that Raman microscopy could become a powerful new tool in pathology.

AUTHOR INFORMATION

Corresponding Author

*Alan Campion, Campion Consulting, LLC, 1887 Westlake Drive, Austin, TX 78746 campion@mail.utexas.edu

Present Addresses

†Dr. Godleski is retired from his hospital and Harvard positions.
‡Dr. Smith is now affiliated with Microtrace LLC, 790 Fletcher Drive, Suite 106, Elgin IL, 60123.

Author Contributions

The manuscript was written through contributions of all authors. All authors have given approval to the final version of the manuscript.

Notes

Declaration of Potential Conflicts of Interest: Alan Campion and John J. Godleski have served as consultants and provided expert testimony in talc and other environmental litigation. Campion Consulting, LLC and John J. Godleski M.D., PLLC are sole proprietorship companies, each with no full-time employees, and less than 5 part-time employees. Kenneth J. Smith is an Employee of Renishaw, Inc. Other co-authors have no potential conflicts to declare.

ACKNOWLEDGEMENTS

This study was supported in part by a pilot project grant (Dr. Fedulov, PI) and the Particles Research Core (Dr. Godleski) of the Harvard Center for Environmental Health supported by NIEHS ES-000002. The authors are grateful for the instrument time generously provided by Renishaw Inc. and for the assistance of Dr. Tim Prusnick and Dr. Richard Bormett in facilitating this collaboration and contributing their scientific expertise to the project. They are also grateful to Dr. Vincent Lynch of The University of Texas at Austin for generating the image shown in Figure 3 and to Dr. Merlin Méheut of GET, Paul-Sabatier University, Toulouse for providing animations of the DFT calculations.

REFERENCES

1. Wolman, M. *J. Histochem. Cytochem.* 1975, 23(1), 21-50.
2. Godleski, J.J. The pneumoconiosis: Silicosis and silicatosis due to inhalation of non-asbestos silicates. In: *Pathology of Pulmonary Disease*; Saldana, M.J., Ed.; J.B. Lippincott Co: 1994; pp 387-393.
3. Abraham, J.L. Analysis of fibrous and non-fibrous particles. In: *Environmental and Occupational Medicine 4th edition*; Rom, W.N.; Markowitz, S.B., Eds.; Lippincott Williams & Wilkins: Philadelphia, 2006; pp 277-297.
4. Shelburne, J.D.; Estrada H.; Hale M.; Ingram, P.; Tucker, J.A. Correlative microscopy and microprobe analysis in pathology. In: *Proceedings of the 47th Annual Meeting of the Electron Microscopy Society of America*. San

Francisco, 1989; Bailey, G.W., ED.; San Francisco: San Francisco Press, 1989:900.
5. Stearns, R.C.; Guttmann, C.R.G.; Bakshi, R.; DeGirolami, U.; Due, B.; Godleski, J.J.;Microsc. Microanal. 2004,10, 1342-1343.
6. Faergemann, J.; Godleski, J.; Laufen, H.;Liss, R.H.; *Acta Derm. Venereol* 1995, *75*, 361-363.
7. Brain, J.D.; Godleski, J.J.; Kreyling, W.G. *Environ Health Perspect*. 1994,*102*(*S5*), 119-125.
8. Cramer, D.W.; Welch, W.R.; Berkowitz, R.S.; Godleski, J.J. *Obstet Gynecol.* 2007, 110, 498-501.
9. Saieg, M.T.A.; Cury, P.M.; Godleski, J.J.; Stearns, R.; Duarte, L.G.;D'Agostino, L.; Pinto, E.M.;Kahn, H.; Pinot, E.M.;Mauad, T.; Saldiva, P.H.;Bernardi, F.D. *Inhal Toxicol*. 2011, *23*, 459-467.
10. Abraham, J.L.; Thackral, C. *Microscopy*. 2007, *56*, 181-187.
11. Larkin, P. Infrared and Raman Spectroscopy: Principles and Spectral Interpretation; Elsevier, Amsterdam, 2011
12. Ferraro, J.R.; Nakamoto, K.; Brown, C. W. *Introductory Raman Spectroscopy 2nd Edition*; Academic Press, Elsevier Science: Amsterdam, 2002.
13. Pence, I,; Mahadevan-Jansen, A. *Chem. Soc. Rev.* 2016, *45*, 1958-1979.
14. Rinaudo, C.;Croce, A.; Musa, M.;Fornero, E.; Allegrina, M.; Trivero, P.; Bellis, D.; Sferch, D.;Toffalorio, F.; Veronsei, G. *Appl. Spectrosc.* 2010, *64*, 571-577.
15. Musa, M.; Croce, A. ; Allegrina, M.; Rinaudo, C.; Belluso, E.; Bellis, D.; Toffalorio, F.; Versonsi, G. *Vib. Spectrosc* 2012, *61*, 66-71.
16. Handbook of Minerals Raman Spectra, Laboratoire de géologie de Lyon, CNRS, ENS de Lyon. http://www.geologie-lyon.fr/Raman/. (Accessed August 2, 2017).
17. Ishii, M.; Shimanouchi, T.; Nakahira, M. *Inorg. Chim. Acta*. 1967, *1*, 387–392.
18. Rosasco, G.J.; Blaha, J.J.,*Appl. Spectrosc.* 1980, *34*, 140–144.
19. Méheut, M.; Schauble, E.A. *Geochim. Cosmochim. Acta* 2014, *134*, 137-154.
20. Wang, M.; Freeman, J.J.; Joliff, B.L. *J. Raman Spectrosc.* 2015, *46*, 829–845.
21. Lafuente, B.; Downs, R.T. Yang, H.; Stone The power of databases: the RRUFF project. In: *Highlights in Mineralogical Crystallography*; Armbruster, T.; Danisi, R.M., Eds.; W. De Gruyter: Berlin 2005; 1-30
22. William, K.P.J.; Nelson. J.; Dyer, S. *The Renishaw Raman database of gemological and mineralogical materials*; Renishaw Transducers System, Gloucestershire, England, 1997.
23. Lovins Micro-Slide Field Finder, Electron Microscopy Sciences, Hatfield, PA 19440

Insert Table of Contents artwork here

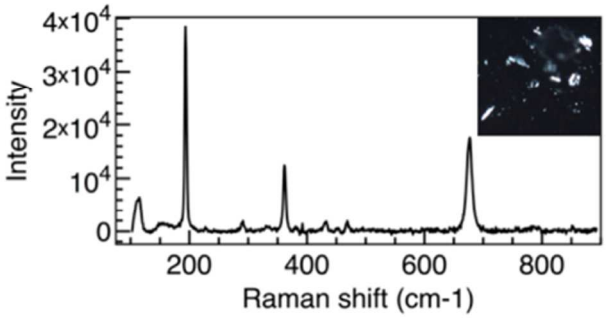
4x10^4
3x10^4
2x10^4
10^4
0
Intensity
200
400
600
800
Raman shift (cm-1)